

# Pushing thermal conductivity to its lower limit in crystals with simple structures

ZeZhu Zeng,<sup>1,2,3,\*</sup> Xingchen Shen,<sup>4,3</sup> Ruihuan Cheng,<sup>1</sup> Olivier Perez,<sup>4</sup> Niuchang Ouyang,<sup>1</sup>  
Zheyong Fan,<sup>5</sup> Pierric Lemoine,<sup>6</sup> Bernard Raveau,<sup>4</sup> Emmanuel Guilmeau,<sup>4,†</sup> and Yue Chen<sup>1,‡</sup>

<sup>1</sup>Department of Mechanical Engineering, The University of Hong Kong, Pokfulam Road, Hong Kong SAR, China

<sup>2</sup>The Institute of Science and Technology Austria, Am Campus 1, 3400 Klosterneuburg, Austria

<sup>3</sup>These authors contributed equally to this work

<sup>4</sup>CRISMAT, CNRS, Normandie Univ, ENSICAEN, UNICAEN, 14000 Caen, France

<sup>5</sup>College of Physical Science and Technology, Bohai University, Jinzhou 121013, China

<sup>6</sup>Institut Jean Lamour, UMR 7198 CNRS – Université de Lorraine, 54011 Nancy, France

(Dated: October 4, 2023)

Materials with low thermal conductivity usually have complex crystal structures. Herein we experimentally find that a simple crystal structure material  $\text{AgTlI}_2$  (I4/mcm) owns an extremely low thermal conductivity of 0.25 W/mK at room temperature. To understand this anomaly, we perform in-depth theoretical studies based on *ab initio* molecular dynamics simulations and anharmonic lattice dynamics. We find that the unique atomic arrangement and weak chemical bonding provide a permissive environment for strong oscillations of Ag atoms, leading to a considerable rattling behavior and giant lattice anharmonicity. This feature is also verified by the experimental probability density function refinement of single-crystal diffraction. The particularly strong anharmonicity breaks down the conventional phonon gas model, giving rise to non-negligible wavelike phonon behaviors in  $\text{AgTlI}_2$  at 300 K. Intriguingly, unlike many strongly anharmonic materials where a small propagative thermal conductivity is often accompanied by a large diffusive thermal conductivity, we find an unusual coexistence of ultralow propagative and diffusive thermal conductivities in  $\text{AgTlI}_2$  based on the thermal transport unified theory. This study underscores the potential of simple crystal structures in achieving low thermal conductivity and encourages further experimental research to enrich the family of materials with ultralow thermal conductivity.

## INTRODUCTION

Pushing the lattice thermal conductivity ( $\kappa$ ) of materials to a lower limit [1, 2] has attracted extensive attention in both condensed matter physics and materials science [3, 4] as it is crucial to promote applications of thermal insulation and thermoelectrics [5, 6]. Phonon, as a collective thermal excitation, plays a crucial role in the heat transport of solid crystals. Therefore, effectively impeding the phonon transport can significantly decrease the  $\kappa$  of solids.

There are two main mechanisms to scatter phonons in semiconductors and insulators: intrinsic phonon-phonon interactions and extrinsic phonon scatterings from phonon-impurity or phonon-boundary interactions. Significant intrinsic phonon-phonon scatterings usually exist in materials with complex crystal structure [7, 8] and strong lattice anharmonicity [9]. Examples of low  $\kappa$  materials at room temperature include  $\text{Cu}_{12}\text{Sb}_4\text{S}_{13}$  (0.69 W/mK) [7] and  $\text{Cs}_2\text{PbI}_2\text{Cl}_2$  (0.45 W/mK) [10]. However, unified theory developed by Simoncelli et al. [11–15] suggests that complicated crystal structure inevitably introduces considerable non-diagonal  $\kappa$  originated from the wavelike tunneling of adjacent phonons, which noticeably enhances the overall  $\kappa$  of materials and indirectly impedes the progress of  $\kappa$  toward its lower limit.

Extrinsic phonon scatterings from lattice defects, boundaries and distortions provide additional ways to scatter phonons efficiently. Superlattice  $\text{Bi}_4\text{O}_4\text{SeCl}_2$  [16] creatively achieves

the lowest  $\kappa$  of 0.1 W/mK at 300 K along the out-of-plane direction in all bulk inorganic solids, via artificially manufactured orientation-dependent lattice distortion (layered superlattice structure) and the introduction of defects (a 88% density of the theoretical value). However, substantial defects in crystals can influence material properties such as electron mobility, toughness and strength [17]. Moreover, directional manipulation of bond strength and connectivity in  $\text{Bi}_4\text{O}_4\text{SeCl}_2$  can only affect the heat transfer in the corresponding direction, and its in-plane  $\kappa$  (1.0 W/mK at 300 K) is still relatively high.

These aforementioned limitations greatly hinder the development of new materials with ultralow  $\kappa$ . In this case, exploring simple crystal structure compounds (low non-diagonal  $\kappa$ ) with intrinsically ultralow (no artificial modification)  $\kappa$  can be an alternative solution. It has been reported that  $\text{PbTe}$  (2 W/mK) [18],  $\text{InTe}$  (1.0 W/mK) [19],  $\text{TlSe}$  (0.5 W/mK) [20],  $\text{Tl}_3\text{VSe}_4$  (0.30 W/mK) [21] possess low  $\kappa$  at 300 K, which open the door to the discovery of ultralow  $\kappa$  in simple crystal structures.

Herein, we synthesized a simple crystal structure phase  $\text{AgTlI}_2$  (space group I4/mcm; eight atoms in the primitive cell (PC)) and find that it exhibits an exceedingly low  $\kappa$  of 0.25 W/mK at room temperature.  $\text{AgTlI}_2$  was synthesized [39, 40] and found to be an electrical insulator [40], while no measurement of  $\kappa$  has been reported in the literature. We performed single-crystal diffraction refinement and find a considerable negative part of the probability density function for Ag atoms, directly unearthing the strongly anharmonic nature of Ag atoms. Based on the *ab initio* molecular dynamics (AIMD) trajectories at 300 K, a large atomic displacement parameter (ADP) and rattling behavior of Ag atoms are also revealed. These unusual phenomena imply strong lattice an-

\* zzeng@ist.ac.at

† emmanuel.guilmeau@ensicaen.fr

‡ yuechen@hku.hk

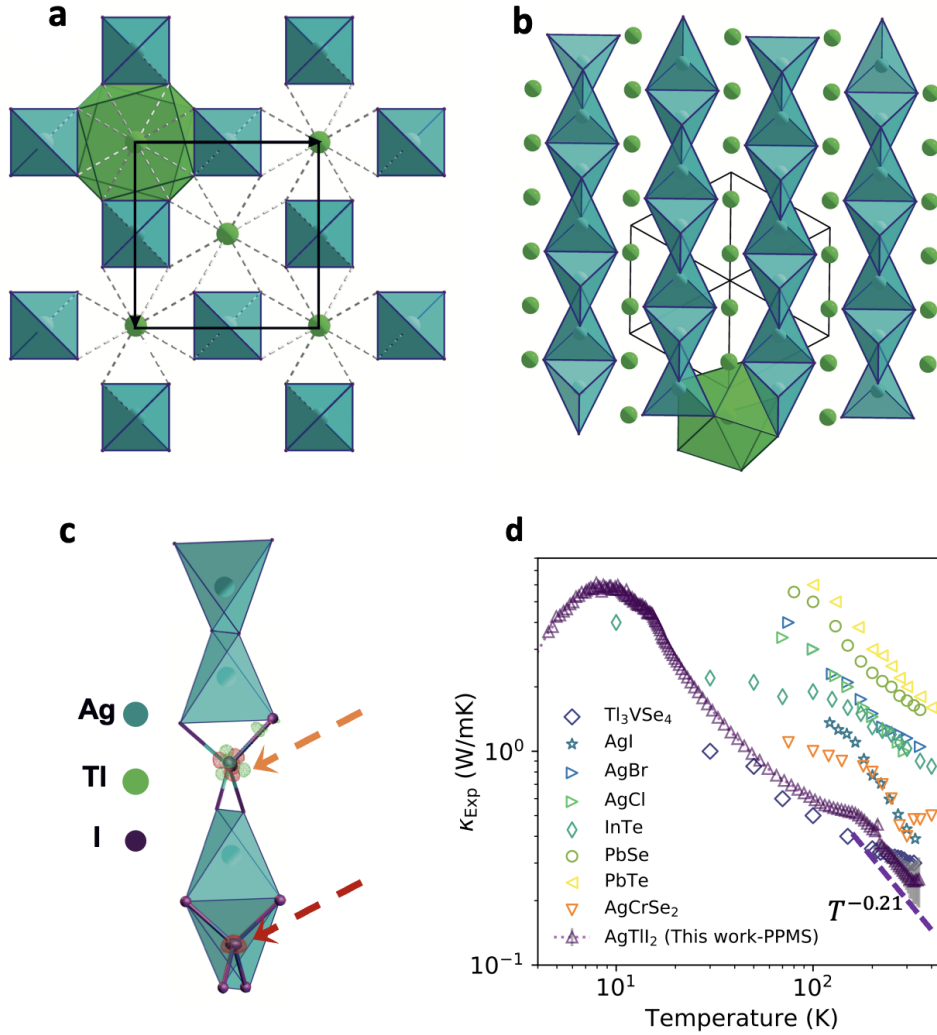


FIG. 1. Structural projection (a) along  $c$ -axis, (b) along  $[111]$  and focus on a  $[\text{AgI}_2]_\infty$  chain. Ag, Tl, and I atoms are drawn using blue, green, and purple circles, respectively. (c) Orange arrow: Residual electron density (red: positive and green: negative) in the area of the Ag site for a harmonic description of Ag. Red arrow: Anharmonic three-dimensional probability density function (pdf) isosurfaces of Ag (red cloud); displacements are pointing toward the faces of the tetrahedron. (d) Experimental thermal conductivity of  $\text{AgTlI}_2$  from 4 to 325 K measured by Physical Property Measurement System (PPMS). Data for  $\text{Tl}_3\text{VSe}_4$  [21],  $\text{AgI}$  [22],  $\text{AgBr}$  [23],  $\text{AgCl}$  [24],  $\text{InTe}$  [19],  $\text{PbSe}$  [25],  $\text{PbTe}$  [25], and  $\text{AgCrSe}_2$  [26, 27] were obtained from previous experiments.

harmonicity in  $\text{AgTlI}_2$ . Using unified theory [13] within the first-principles calculations, we provide further insight into the ultralow  $\kappa$ . In our calculations, a combination of factors is considered, including lattice thermal expansion, temperature-dependent anharmonic force constants [41], phonon frequency renormalization [42, 43] and four [44, 45] phonon scatterings. Our results show that there is a coexistence of suppressed propagative and diffusive heat transfer, uncovering the nature of the ultralow  $\kappa$  in  $\text{AgTlI}_2$ . Based on an in-depth understanding of the heat transport in  $\text{AgTlI}_2$ , we also propose a potential alternative approach to push  $\kappa$  to its lower limit.

## RESULTS AND DISCUSSION

### Experiments

$\text{AgTlI}_2$  and  $\text{AgTl}_2\text{I}_3$  both belong to AgI-TlI quasi-binary silver-thallium iodides system, and they constitute an adjacent regime of the Ag-Tl-I equilibrium phase diagram [39], which inevitably leads to the formation of these two phases during material synthesis. Here, we conducted a low-temperature long-time annealing process in sealed tubes at 373 K to synthesize high-purity sample (see Methods section). Rietveld refinement of the powder X-ray diffraction pattern (PXRD) of the as-synthesized powder (see Fig. S1 of Supplementary Information (SI)) confirms the high purity of our sample, with only traces of  $\text{AgTl}_2\text{I}_3$ .

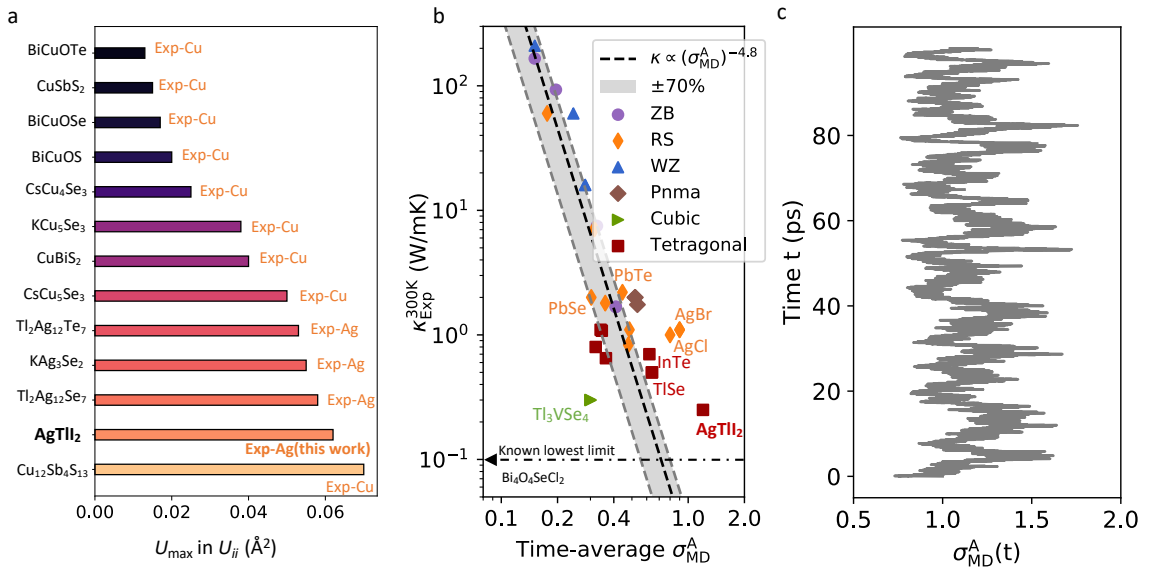


FIG. 2. (a) The maximum ADP ( $U_{\max}$ ) at 300 K in experiments for rattling Cu/Ag atoms in  $\text{AgTlI}_2$  and typical thermoelectric materials [7, 28–35]. (b) Relation between anharmonic parameter ( $\sigma^A$ ) [36, 37] and experimental  $\kappa$  [36–38] of typical simple crystals at 300 K. The data can be found in Table S4 of Supplementary Information. (c) Time dependent anharmonic parameter  $\sigma^A$  of  $\text{AgTlI}_2$  calculated from AIMD simulations at 300 K.

The crystal structure of  $\text{AgTlI}_2$  was established by Flahaut et al. [46]. Here, we performed single crystal diffraction refinement (see Methods for the preparation and characterization) and we confirm that tetragonal crystal structure of this iodide (Fig. 1a-b) has a strong one-dimensional character. It consists of infinite  $[\text{AgI}_2]^-$  chains of edge-sharing  $\text{AgI}_4$  tetrahedrons running along  $c$ -axis. These anionic chains are isolated one from the other and the cohesion of the structure is ensured by the presence of  $\text{Tl}^+$  cations between them (Fig. 1a-b). We demonstrate from this single crystal study that  $\text{Ag}^+$  exhibits a strongly anisotropic vibration inside “I4” tetrahedron. The latter is characterized by maximum quadratic displacement of  $0.056 \text{ \AA}^2$ , corresponding to a maximum vibration of  $0.24 \text{ \AA}$  around its equilibrium position. Importantly, the refined residual electron density around the Ag site in Fig. 1c using harmonic description (see Methods for the details) reveals the presence of significant negative and positive parts of residues around the silver atom, suggesting the invalidation of the harmonic description for Ag atoms. In Fig. 1c, the absence of the negative part of the probability density function (pdf) of Ag atoms by the introduction of third-order Gram-Charlier anharmonic atomic displacement parameter (ADP) (see Methods for details), further indicates the largely anharmonic nature of Ag atoms. The refined crystallographic data and anisotropic ADP ( $U_{ii}$ ) of the single-crystal  $\text{AgTlI}_2$  at 300 K can be found in Table S1 and S2, respectively. Note that, in contrast to Ag, Tl and I elements exhibit distinctly lower ADP.

In order to experimentally determine the thermal conductivity, the as-synthesized powder was densified by Spark Plasma Sintering (SPS, see Methods section for details). Rietveld refinement of the PXRD pattern of the SPS-ed powder (see Fig. S2) confirms that the tetragonal crystal structure of the compound and the high purity of the sample are retained af-

ter sintering. Only traces of  $\text{AgTl}_2\text{I}_3$  with a minor percentage ( $< 1\%$ ) is detected. The refined crystallographic data of  $\text{AgTlI}_2$  and  $\text{AgTl}_2\text{I}_3$  phases are shown in Table S3 of SI. This minor secondary phase makes a negligible contribution of  $\kappa$  to the bulk sample. The temperature ( $T$ ) dependence of the thermal conductivity from 4 to 325 K, displayed in Fig. 1d, shows an extremely low  $\kappa$  of  $0.25 \text{ W/mK}$  at 300 K and features a crystalline peak of  $\kappa$  at an ultralow temperature of 8 K. Moreover,  $\text{AgTlI}_2$  sample follows an unconventional and weak temperature-dependent  $T^{-0.21}$  relation of  $\kappa$  from 100 to 325 K, indicating an anomalous lattice dynamics and thermal transport mechanism. A comparison of the thermal conductivity of  $\text{AgTlI}_2$  with representative materials featuring simple crystal structures (Fig. 1d) further reveals that  $\text{AgTlI}_2$  exhibits at room temperature one of the lowest thermal conductivity among them.

### Molecular dynamics simulations

Bearing in mind from previous studies of low  $\kappa$  compounds, such as  $\text{TlSe}$  [20] and  $\text{Tl}_3\text{VS}_4$  [21], that Tl atoms usually exhibit highly anharmonic vibrations, we perform AIMD simulations using the VASP package [47, 48] to investigate the atomic vibrations. The significant anisotropic atomic displacement parameters (ADPs)  $U_{ii}$  ( $i = 1, 2, 3$ ), displayed in Fig. S6, from 100 to 300 K based on the AIMD atomic trajectories (illustrated in Fig. S5), reveal the magnitude of atomic thermal motion. Strikingly, we find that the ADPs of Ag atoms are significant with nonlinear enhancement from 100 K to 300 K. The magnitudes of  $U_{ii}$  for Tl and I atoms are also smaller than that of Ag atoms with a much linear thermal evolution. The results confirm the single crystal diffraction experimental

data and reveal the strong anharmonicity of Ag ions in AgTlI<sub>2</sub>. Previous studies have attributed the low  $\kappa$  in TlSe [20] and Tl<sub>3</sub>VS<sub>4</sub> [21] to highly anharmonic vibrations of Tl atoms. In AgTlI<sub>2</sub>, Ag atoms show larger oscillations than Tl at 300 K, which indicates the ultralow  $\kappa$  of AgTlI<sub>2</sub> may be more related to Ag element.

In Fig. 2a, we compare the maximum experimental  $U_{ii}$  values between Ag element in AgTlI<sub>2</sub> and Cu and Ag elements (typical rattlers) in thermoelectric materials with ultralow  $\kappa$  at 300 K. The comparison clearly illustrates that the oscillation of Ag atoms in AgTlI<sub>2</sub> surpasses that of most rattling atoms in typical low  $\kappa$  materials. The  $U_{\max}$  in AgTlI<sub>2</sub> is even comparable to the  $U_{\max}$  of Cu in three-fold coordination encountered in tetrahedrite Cu<sub>12</sub>Sb<sub>4</sub>S<sub>13</sub> [49]. These unique features further highlight the strong lattice anharmonicity of AgTlI<sub>2</sub>.

Knoop et al. proposed a parameter ( $\sigma^A$ ) [36, 37] to quantitatively evaluate the degree of lattice anharmonicity as

$$\sigma^A(T) \equiv \frac{\sigma[F^A]_T}{\sigma[F]_T} = \sqrt{\frac{\sum_{i,\alpha} \langle (F_{i,\alpha}^A)^2 \rangle_T}{\sum_{i,\alpha} \langle (F_{i,\alpha})^2 \rangle_T}}, \quad (1)$$

where  $i$ ,  $\alpha$  and  $T$  are respectively the atomic index, Cartesian direction and temperature.  $F^A$  and  $F$  represent the anharmonic and total atomic forces, respectively. Note that  $\sigma^A$  is time dependent in AIMD simulations, and we can derive its time average readily. For most materials with modest anharmonicity, it will converge rapidly with the increase of simulation time [36, 37]. We computed (see Methods for details) the  $\sigma^A$  of AgTlI<sub>2</sub> and some typical crystals (Tl<sub>3</sub>VSe<sub>4</sub>, TlSe, PbTe, PbSe, AgCl and AgBr) with simple crystal structures and ultralow  $\kappa$  at 300 K from AIMD simulations, and make a comparison (Fig. 2b) with the  $\kappa$ - $\sigma^A$  power-law model proposed by Knoop et al. [36, 37]. All harmonic atomic forces are computed using the finite displacement method [50].

It is found that AgTlI<sub>2</sub> owns the largest time-average  $\sigma^A$  among these materials and significantly deviates from the power-law model at 300 K, which are the intrinsic imprints of its large atomic displacement parameters and strong lattice anharmonicity, further implying its ultralow  $\kappa$ . We note that the calculated  $U_{\max}$  for Ag in AgTlI<sub>2</sub> at 300 K (0.097 Å<sup>2</sup>) based on AIMD trajectories is larger than that of our experiments (0.061 Å<sup>2</sup>), which may be used to rationalize the significant deviation of  $\sigma^A$  from the power-law model. Moreover, the time evolution (Fig. 2c) of  $\sigma^A$  of AgTlI<sub>2</sub> shows pronounced fluctuations in a period of several picoseconds, a behavior not observed in other materials with similar crystal structures, such as InTe (see Fig. S7). Knoop et al. [37] reported the hopping of  $\sigma^A$  in CuI and KCaF<sub>3</sub>, which can be ascribed to the formation of some metastable defect geometries. However, the intrinsic mechanism is different here; there is no metastable structure formed in AgTlI<sub>2</sub>. A fluctuation of  $\sigma^A$  was also reported by Knoop et al. [36] in rock-salt AgBr at 300 K, a well-known ionic conductor [51]. Fortunately, our experimental measurements do not indicate any superionic diffusion or ionic thermal conductivity in AgTlI<sub>2</sub>, which contributes to the stability of an exceptionally low  $\kappa$  in AgTlI<sub>2</sub>.

## Anharmonic lattice dynamics

Atomic vibrations can be directly observed in MD simulation, while it is nontrivial to obtain more insights into the microscopic phonon transport mechanisms. Thus, we further study the anharmonic lattice dynamics within the perturbation theory (PT) on the basis of first-principles calculations. According to the unified theory [13], the lattice thermal conductivity can be written as

$$\kappa = \frac{\hbar^2}{k_B T^2 V N_{\mathbf{q}}} \sum_{\mathbf{q}} \sum_{j,j'} \frac{\omega_{\mathbf{q}}^j + \omega_{\mathbf{q}}^{j'}}{2} \mathbf{v}_{\mathbf{q}}^{j,j'} \otimes \mathbf{v}_{\mathbf{q}}^{j',j} \cdot \frac{\omega_{\mathbf{q}}^j n_{\mathbf{q}}^j (n_{\mathbf{q}}^j + 1) + \omega_{\mathbf{q}}^{j'} n_{\mathbf{q}}^{j'} (n_{\mathbf{q}}^{j'} + 1)}{4 (\omega_{\mathbf{q}}^{j'} - \omega_{\mathbf{q}}^j)^2 + (\Gamma_{\mathbf{q}}^j + \Gamma_{\mathbf{q}}^{j'})^2} (\Gamma_{\mathbf{q}}^j + \Gamma_{\mathbf{q}}^{j'}), \quad (2)$$

where  $T$ ,  $\hbar$ ,  $k_B$ ,  $V$  and  $N_{\mathbf{q}}$  are respectively the temperature, reduced Planck constant, the Boltzmann constant, the volume of the unit cell, and the total number of wave vectors.  $\mathbf{v}_{\mathbf{q}}^{j,j'}$ ,  $\Gamma_{\mathbf{q}}^j$  and  $\omega_{\mathbf{q}}^j$  are respectively group velocity, linewidth and frequency of a specific phonon with wave vector  $\mathbf{q}$  and branches  $j$  and  $j'$ . When  $j = j'$ , Eq. 2 computes the conventional propagative thermal conductivity ( $\kappa_{\text{pg}}$ ), and if  $j \neq j'$ , it calculates the diffusive thermal conductivity ( $\kappa_{\text{diff}}$ ).

Eq. 2 indicates that phonon frequency  $\omega$  and linewidth  $\Gamma$  are two crucial factors that determine  $\kappa$ . Therefore, a sophisticated treatment to these parameters is necessary for strongly anharmonic system. We consider a combination of factors including: lattice thermal expansion, temperature-dependent phonon frequency renormalization [42, 43, 55] and four-phonon interactions [44, 45]. We carefully compare the effects of these factors on the phonon frequencies and linewidths (see Fig. S8 and S9) of AgTlI<sub>2</sub> at 300 K, and find that all of them are important to reliably understand the  $\kappa$  of AgTlI<sub>2</sub>.

In Figs. 3a and 3b,  $\kappa_{\text{pg}}$  and  $\kappa_{\text{diff}}$  calculated using different combinations of phonon frequencies and linewidths are reported at 300 K. First, we find that lattice thermal expansion (TE) can largely decrease the  $\kappa_{\text{pg}}$ , as the TE significantly softens the low-frequency phonons and enhances the phonon scatterings (see Figs. S8 and S9). The enhancement of low-frequency phonon linewidths is strongly related to the stronger couplings of low-frequency acoustic and optical phonon modes as these softened phonons have a wider energy distribution and thus easier to satisfy the energy conservation after considering TE. Interestingly, the  $\kappa_{\text{pg}}$  is enhanced markedly when phonon frequency renormalization is considered via the temperature-dependent effective potential (TDEP) scheme [42, 43]. In fact, this phenomenon was also reported in previous studies [7, 10] as the low-frequency phonons (main heat carriers) are hardened significantly (see Fig. S8) due to the high-order anharmonic renormalization and thus weakening of phonon interactions. By contrast,  $\kappa_{\text{diff}}$  is not as sensitive as  $\kappa_{\text{pg}}$  over TE and frequency renormalization. With these necessary considerations, the predicted overall thermal conductivity ( $\kappa_{\text{pg}} + \kappa_{\text{diff}}$ ) agrees well with the experiments.

Comparing the spectral- $\kappa$  with respect to the phonon frequency as shown in Figs. 3c and 3d, we see that the low-

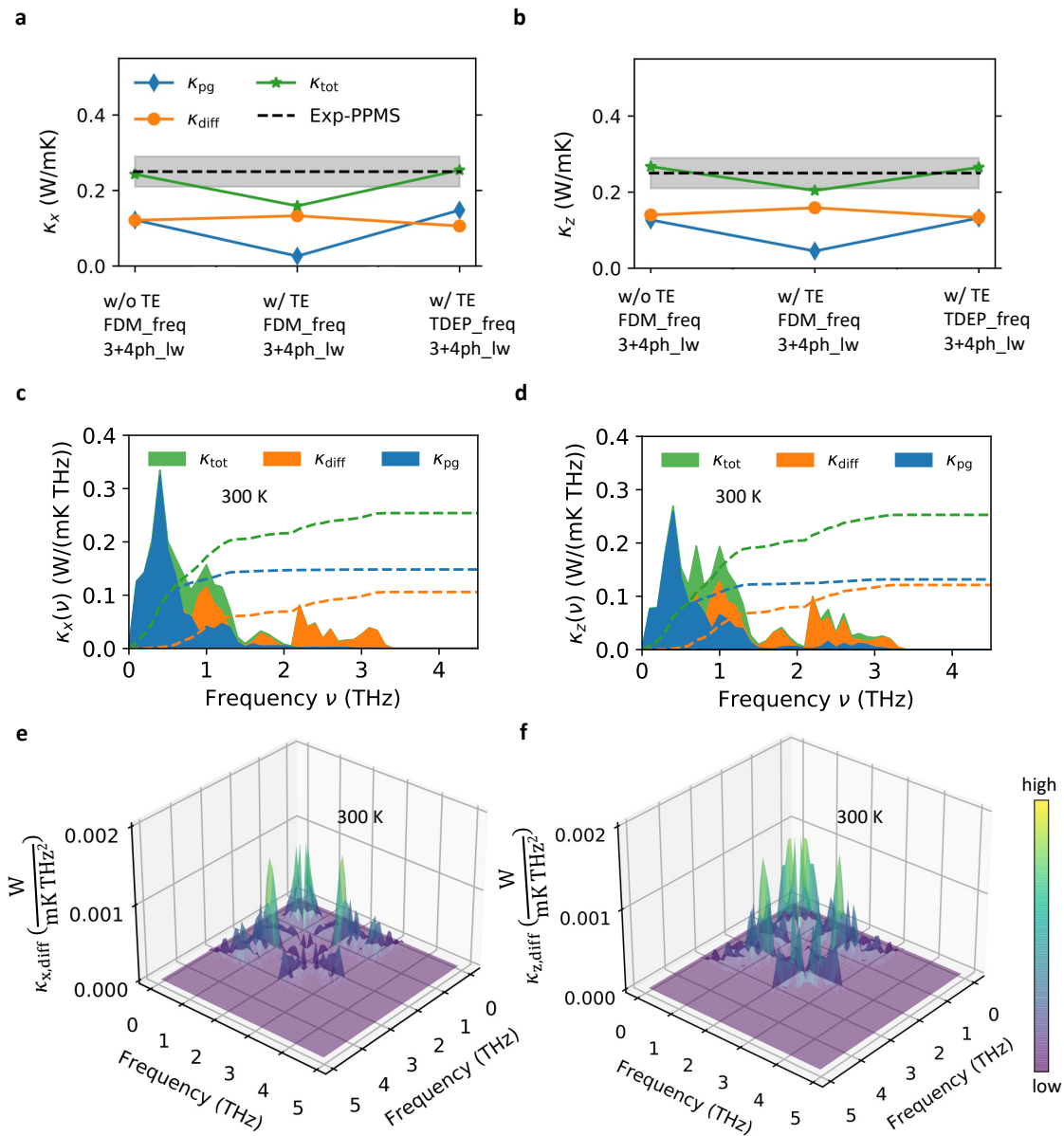


FIG. 3. Lattice thermal conductivities of  $\text{AgTlI}_2$  calculated at 300 K along  $x$  (a) and  $z$  (b) directions using three different sets of phonon properties extracted from perturbation theory. Solid lines are guide for eyes. TE represents thermal expansion. Phonon frequencies (freq) have been extracted from finite displacement method (FDM) [50] and the temperature-dependent effective potential (TDEP) scheme [42, 43]. For phonon linewidths (lw), three- [52] and four-phonon interactions [44, 45] are included. Experimental results (black dashed line) with measurement uncertainty (gray shaded area) are shown. Two-channel spectral lattice thermal conductivities ( $\kappa_{pg}$  and  $\kappa_{diff}$ ) calculated using the unified theory [13] at 300 K (using TDEP phonon frequency and 3+4ph\_lw) along  $x$  (c) and  $z$  (d) directions, and the three-dimensional frequency-plane distribution of  $\kappa_{diff}$  along  $x$  (e) and  $z$  (f) directions.

frequency phonons (0~1 THz) have significant contributions to the propagative thermal transport. From the phonon density of states at 300 K (see Fig. S10), we know that these phonons are mainly dominated by the vibrations of Tl atoms. The diffusive thermal transport can be greatly contributed by the phonons in the frequency ranges of 0.8~1.5 and 2~3 THz, and these phonons are strongly related to Ag atoms as revealed by phonon density of states (see Fig. S10). Based on the three-dimensional distribution of  $\kappa_{diff}$  as shown in Figs. 3e

and 3f, it is also apparent that wavelike tunnelings between low-frequency (~1 THz) and high-frequency phonon modes (2~3 THz) can considerably contribute to the diffusive thermal transport. Combined phonon density of states with spectral- $\kappa$ , we conclude that the strong oscillation and anharmonicity of Ag atoms lead to two crucial thermal transport features in  $\text{AgTlI}_2$ : (i) dramatically scattered high-frequency phonons and effectively decreased  $\kappa_{pg}$ ; (ii) glass-like thermal transport and non-negligible  $\kappa_{diff}$ . With weak atomic bonding and sim-

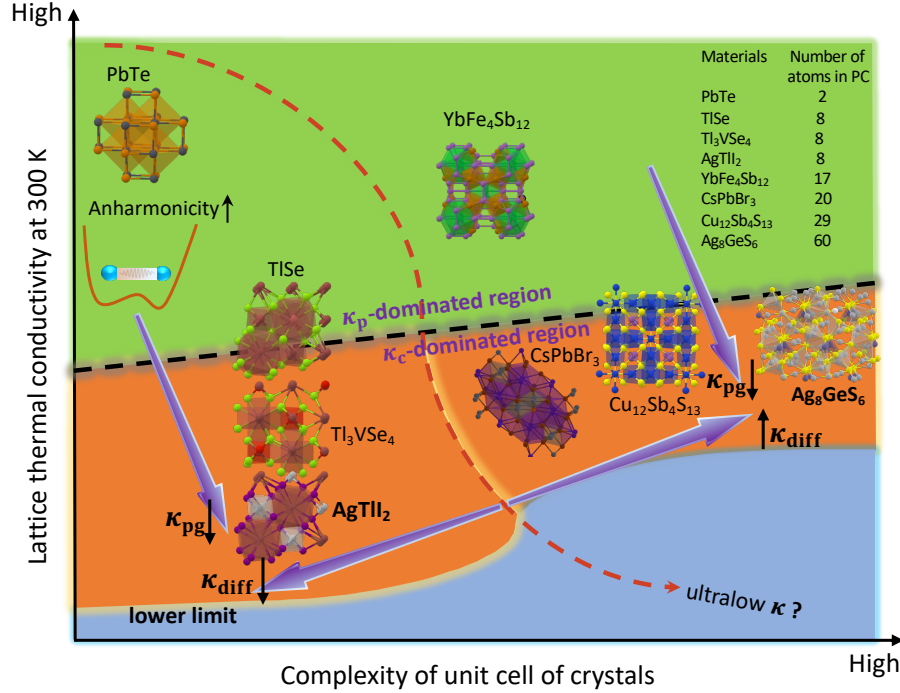


FIG. 4. Illustration of potential pathways for pushing  $\kappa$  to its lower limit in inorganic materials. We define the complexity of crystals based on the number of atoms in a primitive cell. Lattice thermal conductivities are extracted from previous studies based on unified theory [7, 13, 53, 54]. We compute the two-channel  $\kappa$  of  $\text{AgTlI}_2$  and  $\text{Ag}_8\text{GeS}_6$  in this work.

ple crystal structure,  $\text{AgTlI}_2$  avoids severe phonon bunching and achieves a coexistence of both ultralow  $\kappa_{\text{pg}}$  and  $\kappa_{\text{diff}}$  at 300 K.

### Pushing low $\kappa$ to a lower limit

The discovery of ultralow- $\kappa$  materials at room temperature in simple and fully dense crystal structure has proven extremely challenging. In Fig. 4, we show a schematic diagram for potential different pathways to find lower  $\kappa$ . A current protocol (red dashed line) for finding ultralow- $\kappa$  materials is enhancing the complexity of materials (here we define the complexity of materials based on the total number of atoms in the PC). Along this line, some complex materials with low  $\kappa$  were found readily such as skutterudite  $\text{YbFe}_4\text{Sb}_{12}$  [54] and perovskite  $\text{CsPbBr}_3$  [5], as complex materials normally possess lower crystal symmetries and stronger phonon couplings. However, under the framework of the two-channel thermal transport, this protocol may not be efficient to suppress  $\kappa$  if there is a non-negligible diffusive heat transport channel ( $\kappa_{\text{diff}}$ ). In contrast, we even see a higher  $\kappa$  when the complexity of materials is raised, such as tetrahedrite  $\text{Cu}_{12}\text{Sb}_4\text{S}_{13}$  [7] and argyrodite  $\text{Ag}_8\text{GeS}_6$ .

$\text{Ag}_8\text{GeS}_6$  (60 atoms in PC) [56] is an excellent example to explain this phenomenon. We compute its  $\kappa_{\text{pg}}$  using unified

theory and find that it is only 0.04 W/mK at 300 K, which is lower than that of  $\text{AgTlI}_2$  and even close to the  $\kappa$  of air (0.025 W/mK at 300 K). Nevertheless, the  $\kappa_{\text{diff}}$  is equal to 0.43 W/mK and it is much higher than  $\kappa_{\text{pg}}$ , which can be attributed to the severe coherence of phonon modes (180 phonon branches in the first Brillouin zone) with strong lattice anharmonicity (see Fig. S12 for phonon properties and two-channel  $\kappa$  of  $\text{Ag}_8\text{GeS}_6$ ). In other words, although strong lattice anharmonicity in complex materials can dramatically decrease  $\kappa_{\text{pg}}$  (purple arrows in Fig. 4), the total  $\kappa$  can increase due to the high diffusive thermal transport. We highlight that the coexistence of ultralow  $\kappa_{\text{pg}}$  and  $\kappa_{\text{diff}}$  is the key to achieve strongly suppressed  $\kappa$ .  $\text{AgTlI}_2$  delivers on both fronts, demonstrating the potential of simple crystal structures with strong lattice anharmonicity to push  $\kappa$  to a lower limit. Therefore, finding materials with simple crystal structures and giant lattice anharmonicity (quantified by  $\sigma^A$  [37]) can be a feasible way to push  $\kappa$  to its lower limit.

Recent studies have focused on finding high thermoelectric  $zT$  values from complex materials [57] and even high-entropy alloys [58]. However, an enhanced  $\kappa$  at elevated temperature was observed in complex materials such as high entropy alloy  $\text{BiSbTe}_{1.5}\text{Se}_{1.5}$  [58] and Zintl compound  $\text{BaAg}_2\text{Te}_2$  (20 atoms in PC) [59]. In fact, these complex materials already show the glass-like heat transport behavior around room temperature (large  $\kappa_{\text{diff}}$ ), similar with  $\text{Ag}_8\text{GeS}_6$ . The increase of  $\kappa$  con-

siderably affects the efficiency of thermal energy conversion at high temperatures. Therefore, this work also highlights the need for continued efforts in finding high-performance thermoelectric materials with simple crystal structures.

## CONCLUSION

We synthesized polycrystalline  $\text{AgTlI}_2$  with a simple crystal structure, and report its ultralow  $\kappa$  at room temperature via both state-of-the-art experiments and calculations. This unusually low value of  $\kappa$  is close to the known lowest limit [16] of any bulk inorganic materials. We thoroughly investigate its thermal transport nature by revealing the large thermal vibrations of Ag atoms from single-crystal diffraction refinements and AIMD simulations, and uncover the origin of simultaneously suppressed particle-like and wave-like phonon thermal transports based on the unified theory. Compared with previous efforts on searching for ultralow  $\kappa$  in complex materials, our work emphasizes the unique advantages and features of simple crystal structures, and also suggests an alternative and practicable way to find new inorganic materials with ultralow thermal conductivity.

## METHODS

*Sample preparation.* The nominal  $\text{AgTlI}_2$  sample was prepared starting from the high-purity precursors AgI (powder, 99.999%) and TlI (ball, 99.999%). Stoichiometric amount of 3g precursors was mixed and loaded into a carbon-coated silica tube inside of the glove-box, followed by sealing and evacuating ( $\sim 10^{-3}$  Pa) under vacuum. The mixture of precursors was melted at 873 K for 24 hours, and then slowly dropped to 373 K over 24 hours, followed by annealing at this temperature for 240 hours. The obtained ingot was hand ground into fine powders. Finally, they were densified by SPS at 373 K under a pressure of 200 MPa for 10 minutes using a 10 mm diameter WC die. The resulting SPS-ed sample has a geometrical density of 6.85 g/cm<sup>3</sup>, i.e., around 99% of the theoretical density.

*X-ray diffraction.* PXRD of the synthesized powder, SPS-ed powder, and consolidated bulk sample were recorded on a PANalytical XPert2 system with Cu  $K_{\alpha 1}/K_{\alpha 2}$  radiation ( $\lambda_1=1.541$  Å,  $\lambda_2=1.544$  Å). Rietveld refinements of PXRD patterns were performed using GSAS (General Structure Analysis System) packages [60]. In Fig. S3, XRD patterns of the bulk sample (surface perpendicular to the SPS pressure direction) has a comparable pattern as that of the SPS-ed powder sample, implying non-preferential orientation in the bulk sample.

The batch synthesis was composed of grains of matter a few tens of micrometers in size. These grains of matter were not single-crystals, and were broken up with a scalpel and selected using a stereomicroscope. They were mounted on microloops and their diffraction quality was tested. After numerous trials and errors, we finally succeeded in isolating a single crystal of the targeted phase of sufficient quality; the dimensions of this crystal were  $0.011 \times 0.008 \times 0.008$  mm<sup>3</sup>. X-ray diffraction

measurement on a single crystal was then performed on Rigaku Synergy S diffractometer, equipped with a micro-focus sealed X-ray Mo tube and an Eiger 1M Dectris photon counting detector. Due to the very small size of the sample, an extremely long exposure time was chosen (360 s/0.5°); the utilization of the measurement strategy enabled us to obtain 97% completeness at a theta angle of 36.9°. Data reduction was performed with CrysAlisPro. The structure determination was then performed using SHELXS3 [61] in the I4/mcm space group and refined using Olex2 [62]. Although the structural refinement was quite satisfactory, the Fourier difference map revealed the presence of significant residues around the silver atom. Four positive residues and four negative residues of equal weight surrounded the silver atom (Fig. 1c), indicating a poor description of this atom. Silver cation with d<sup>10</sup> configuration can easily adopt various complex asymmetric coordination; Ag<sup>+</sup> ions can be observed in different but overlapping sites. The structure is then characterized by the presence of static or dynamic disorders. Whatever the situation, the description of the site is complex and the use of higher order tensor elements to model the ADP [63] can be an elegant solution to this problem.

The Gram-Charlier formalism is recommended by the IUCr Commission on Crystallographic Nomenclature. Note that the anharmonic approach has been successfully used in the past to solve numerous structures, both of nonconducting materials [64] and of fast ion conducting phases [65]. In the present case, the introduction of third-order Gram-Charlier anharmonic ADP for the silver site significantly improved the refinement to R = 1.97 % (against 3.44%) for one additional parameter, with a drop of the residuals in the Fourier difference maps ( $[-0.7 \text{ e}^-/\text{Å}^3 - 1.8 \text{ e}^-/\text{Å}^3]$  against  $[-2.5 \text{ e}^-/\text{Å}^3 - 2.7 \text{ e}^-/\text{Å}^3]$ ) in the harmonic approach. The probability density function (pdf) for the silver site is plotted in Fig. 1c; the absence of negative part in the pdf validates the present model. As already reported by different authors for d<sup>10</sup> elements, the probability density deformation increases the electron density of the Ag site toward the faces of the tetrahedron.

*Thermal transport measurements.* Thermal conductivities of  $\text{AgTlI}_2$  bulk sample were measured from 4 to 325 K using a Physical Property Measurement System (PPMS, Quantum Design, Dynacool 9 T). In order to cross-check  $\kappa$  of  $\text{AgTlI}_2$  obtained from PPMS, we also measured thermal diffusivity and thermal conductivity (see Fig. S4) on a Netzsch LFA 457 laser flash system under a nitrogen atmosphere from 300 to 373 K. The collected data of  $\kappa$  from different apparatus (PPMS and LFA) agreed with each other within experimental error at 300 K, validating the reproducible and trustable ultralow  $\kappa$  of  $\text{AgTlI}_2$  bulk sample. Based on the non-preferential orientation of bulk sample (Fig. S3), we therefore regarded it has isotropic thermal transport property and measured  $\kappa$  without checking the anisotropic property in our experiments. The nearly identical calculated values of  $\kappa_x$  and  $\kappa_z$  (see Fig. 3) also suggest that the variation in thermal conductivity among the three Cartesian directions is slight.

*AIMD simulations.* A  $2 \times 2 \times 2$  supercell with experimental lattice constants at 300 K was used to perform the AIMD simulations with NVT ensemble and obtain the atomic trajectories. An energy cutoff value of 400 eV and a  $\Gamma$ -centered  $1 \times$

$1 \times 1 \times k$ -point mesh were used for AIMD simulations with the PBEsol [66] functional. AIMD trajectory with a time duration of 100 ps was used to visualize the atomic vibration as shown in Fig. S1 and calculate the ADPs. For the calculations of  $\sigma^A$  of PbTe, PbSe, AgCl, AgBr, AgTlI<sub>2</sub>, Tl<sub>3</sub>VSe<sub>4</sub>, InTe and TlSe at 300 K, we performed AIMD simulations of about 10 ps ( $\sigma^A$  has already converged within 10 ps) under the NVT ensemble to obtain the total interatomic forces. For the calculation of  $\sigma^A$ , harmonic interatomic forces were calculated using the finite displacement method implemented in the Phonopy package [50]. The anharmonic interatomic forces were obtained by subtracting the harmonic forces from the total forces. All specific data reported in Fig. 2b can be found in Table S4.

**Interatomic force constants.** Temperature-dependent second-order interatomic force constants (IFCs) were extracted at 300 K using the TDEP [42, 43] scheme developed by Hellman et al., as implemented in the hiPhive package [67]. For the unit cell without the consideration of thermal expansion (w/o TE), the lattice constants were relaxed at 0 K ( $a = 8.24$  Å;  $c = 7.59$  Å). For the unit cell with the thermal expansion (w/ TE), experimental lattice constants ( $a = 8.35$  Å;  $c = 7.66$  Å) at 300 K were used. 80 configurations in AIMD simulations were randomly selected as the training set. We raised the energy cutoff to 500 eV with a denser  $3 \times 3 \times 3$   $k$ -point mesh to perform accurate single-point calculations. We obtained the temperature-dependent cubic and quartic IFCs at 300 K using the hiPhive package [67] and our in-house code. The harmonic terms at 0 K calculated using Phonopy [50] were subtracted from the atomic forces and only cubic and quartic force constants were extracted to the residual force-displacement data. Due to the strong anharmonicity of AgTlI<sub>2</sub>, we expect that higher-than-fourth-order anharmonic terms may also contribute to the residual atomic forces. Therefore, in the fitting process, we further built the atomic force constant potential up to the sixth-order anharmonicity to fit the residual force-displacement data and excluded the disturbances from the fifth- and sixth-order terms to the cubic and quartic IFCs. We compared the fitting performances of atomic force constant potentials based on the different Taylor expansion truncations up to the fourth- or sixth-order (see Fig. S11), and found that including the fifth- and sixth-order anharmonicity can considerably improve the fitting performance. Note that this fitting scheme was also used by Tadano

et al. [68] to reliably extract the third and fourth-order IFCs of strongly anharmonic clathrate Ba<sub>8</sub>Ga<sub>16</sub>Ge<sub>30</sub>.

For AgTlI<sub>2</sub>, we used the converged neighbor cutoff distances 7.5, 6.0 and 4.2 Å to extract the IFCs of second, third and fourth-order terms, respectively. For Ag<sub>8</sub>GeS<sub>6</sub>, a  $2 \times 2 \times 1$  supercell (240 atoms) was used to perform AIMD simulations at 300 K. We then used the same method to extract the second-, third- and fourth-order IFCs at 300 K with cutoff distances of 7.0, 4.0 and 3.0 Å, respectively.

**Lattice thermal conductivity.** Three-phonon linewidths were calculated using the ShengBTE [52] package. Four-phonon linewidths were calculated using our in-house code based on the formulae developed by Feng et al. [44, 45]. We carefully tested the relation between  $q$ -point mesh and  $\kappa$ , and a  $9 \times 9 \times 9$   $q$ -point mesh was used to compute the phonon linewidths and the  $\kappa$  of AgTlI<sub>2</sub>. The scalebroad of Gaussian function in the ShengBTE package was set to 1 and 0.25 for the calculations of the three- and four-phonon scatterings, respectively. For Ag<sub>8</sub>GeS<sub>6</sub>, a  $6 \times 4 \times 3$   $q$ -point mesh was used to compute the  $\kappa$ , and the scalebroad was set to 1 and 0.1 for three- and four-phonon scatterings, respectively.

#### Acknowledgments

We thank Bingqing Cheng (IST Austria) and Terumasa Tadano (NIMS Japan) for reading the manuscript and providing insightful comments. This work is supported by the Research Grants Council of Hong Kong (C7002-22Y and 17318122). ZZ acknowledges the European Union’s Horizon 2020 research and innovation programme under the Marie Skłodowska-Curie grant agreement No. 101034413. XS acknowledges funding from the European Union’s Horizon 2020 research and innovation program under the Marie Skłodowska-Curie grant agreement No. 101034329, and the WINNING-Normandy Program supported by the Normandy Region. The computations were performed using research computing facilities offered by Information Technology Services, the University of Hong Kong.

#### Author contributions

Z.Z., and Y.C. conceived the idea; Z.Z. and Y.C. designed the research; Z.Z., R.C., N.O., and Z.F. performed the calculations; X.S., O.P., P.L., B.R., and E.G. performed the experiments. All authors wrote the paper.

#### Competing interests

The authors declare no competing interests.

- 
- [1] X. Qian, J. Zhou, and G. Chen, “Phonon-engineered extreme thermal conductivity materials,” *Nature Materials* **20**, 1188 (2021).
  - [2] S. E. Kim and D. G. Cahill, “Pushing low thermal conductivity to the limit,” *Science* **373**, 963 (2021).
  - [3] L. Lindsay, C. Hua, X. Ruan, and S. Lee, “Survey of ab initio phonon thermal transport,” *Materials Today Physics* **7**, 106 (2018).
  - [4] R. Hanus, R. Gurunathan, L. Lindsay, M. T. Agne, J. Shi, S. Graham, and G. Jeffrey Snyder, “Thermal transport in defective and disordered materials,” *Applied Physics Reviews* **8**, 031311 (2021).
  - [5] W. Lee, H. Li, A. B. Wong, D. Zhang, M. Lai, Y. Yu, Q. Kong, E. Lin, J. J. Urban, J. C. Grossman, *et al.*, “Ultralow thermal conductivity in all-inorganic halide perovskites,” *Proceedings of the National Academy of Sciences* **114**, 8693 (2017).
  - [6] Q. Yan and M. G. Kanatzidis, “High-performance thermoelectrics and challenges for practical devices,” *Nature Materials* **21**, 503 (2022).
  - [7] Y. Xia, V. Ozoliņš, and C. Wolverton, “Microscopic mechanisms of glasslike lattice thermal transport in cubic Cu<sub>12</sub>Sb<sub>4</sub>S<sub>13</sub> tetrahedrites,” *Physical Review Letters* **125**, 085901 (2020).
  - [8] R. Hanus, J. George, M. Wood, A. Bonkowski, Y. Cheng, D. L. Abernathy, M. E. Manley, G. Hautier, G. J. Snyder, and R. P.



- Hermann, “Uncovering design principles for amorphous-like heat conduction using two-channel lattice dynamics,” *Materials Today Physics* **18**, 100344 (2021).
- [9] C. W. Li, J. Hong, A. F. May, D. Bansal, S. Chi, T. Hong, G. Ehlers, and O. Delaire, “Orbitally driven giant phonon anharmonicity in SnSe,” *Nature Physics* **11**, 1063 (2015).
- [10] Z. Zeng, C. Chen, C. Zhang, Q. Zhang, and Y. Chen, “Critical phonon frequency renormalization and dual phonon coexistence in layered ruddlesden-popper inorganic perovskites,” *Physical Review B* **105**, 184303 (2022).
- [11] P. B. Allen and J. L. Feldman, “Thermal conductivity of glasses: Theory and application to amorphous Si,” *Physical Review Letters* **62**, 645 (1989).
- [12] P. B. Allen and J. L. Feldman, “Thermal conductivity of disordered harmonic solids,” *Physical Review B* **48**, 12581 (1993).
- [13] M. Simoncelli, N. Marzari, and F. Mauri, “Unified theory of thermal transport in crystals and glasses,” *Nature Physics* **15**, 809 (2019).
- [14] L. Isaeva, G. Barbalinardo, D. Donadio, and S. Baroni, “Modeling heat transport in crystals and glasses from a unified lattice-dynamical approach,” *Nature Communications* **10**, 1 (2019).
- [15] M. Simoncelli, N. Marzari, and F. Mauri, “Wigner formulation of thermal transport in solids,” *Physical Review X* **12**, 041011 (2022).
- [16] Q. D. Gibson, T. Zhao, L. M. Daniels, H. C. Walker, R. Daou, S. Hébert, M. Zanella, M. S. Dyer, J. B. Claridge, B. Slater, *et al.*, “Low thermal conductivity in a modular inorganic material with bonding anisotropy and mismatch,” *Science* **373**, 1017 (2021).
- [17] A. Shekhawat and R. O. Ritchie, “Toughness and strength of nanocrystalline graphene,” *Nature Communications* **7**, 10546 (2016).
- [18] Z. Tian, J. Garg, K. Esfarjani, T. Shiga, J. Shiomi, and G. Chen, “Phonon conduction in PbSe, PbTe, and PbTe<sub>1-x</sub>Se<sub>x</sub> from first-principles calculations,” *Physical Review B* **85**, 184303 (2012).
- [19] J. Zhang, N. Roth, K. Tolborg, S. Takahashi, L. Song, M. Bondesgaard, E. Nishibori, and B. B. Iversen, “Direct observation of one-dimensional disordered diffusion channel in a chain-like thermoelectric with ultralow thermal conductivity,” *Nature Communications* **12**, 1 (2021).
- [20] M. Dutta, S. Matteppanavar, M. V. Prasad, J. Pandey, A. Warankar, P. Mandal, A. Soni, U. V. Waghmare, and K. Biswas, “Ultralow thermal conductivity in chain-like TlSe due to inherent Tl<sup>+</sup> rattling,” *Journal of the American Chemical Society* **141**, 20293 (2019).
- [21] S. Mukhopadhyay, D. S. Parker, B. C. Sales, A. A. Puretzy, M. A. McGuire, and L. Lindsay, “Two-channel model for ultralow thermal conductivity of crystalline Tl<sub>3</sub>VSe<sub>4</sub>,” *Science* **360**, 1455 (2018).
- [22] Y. Wang, Q. Gan, M. Hu, J. Li, L. Xie, and J. He, “Anharmonic lattice dynamics and the origin of intrinsic ultralow thermal conductivity in AgI materials,” *Physical Review B* **107**, 064308 (2023).
- [23] K. Kamran, M. Anis-ur Rehman, and A. Maqsood, “Thermal and electrical properties of crystalline silver bromide,” *Journal of Physics D: Applied Physics* **40**, 869 (2007).
- [24] A. Maqsood, M. Anis-ur Rehman, K. Kamran, and I. H. Gul, “Thermophysical properties of AgCl in the temperature range 77-300 k,” *Journal of Physics D: Applied Physics* **37**, 1845 (2004).
- [25] N. Shulumba, O. Hellman, and A. J. Minnich, “Intrinsic localized mode and low thermal conductivity of PbSe,” *Physical Review B* **95**, 014302 (2017).
- [26] F. Damay, S. Petit, S. Rols, M. Braendlein, R. Daou, E. Elkaim, F. Fauth, F. Gascoin, C. Martin, and A. Maignan, “Localised Ag<sup>+</sup> vibrations at the origin of ultralow thermal conductivity in layered thermoelectric AgCrSe<sub>2</sub>,” *Scientific Reports* **6**, 23415 (2016).
- [27] F. Gascoin and A. Maignan, “Order-disorder transition in AgCrSe<sub>2</sub>: A new route to efficient thermoelectrics,” *Chemistry of Materials* **23**, 2510 (2011).
- [28] Y. Mizuguchi, A. Miura, A. Nishida, O. Miura, K. Tadanaga, N. Kumada, C. Lee, E. Magome, C. Moriyoshi, and Y. Kuroiwa, “Compositional and temperature evolution of crystal structure of new thermoelectric compound LaOBiS<sub>2-x</sub>Se<sub>x</sub>,” *Journal of Applied Physics* **119**, 155103 (2016).
- [29] S. O. Long, A. V. Powell, S. Hull, F. Orlandi, C. C. Tang, A. R. Supka, M. Fornari, and P. Vaqueiro, “Jahn–teller driven electronic instability in thermoelectric tetrahedrite,” *Advanced Functional Materials* **30**, 1909409 (2020).
- [30] P. Vaqueiro, R. A. R. Al Orabi, S. D. Luu, G. Guelou, A. V. Powell, R. Smith, J.-P. Song, D. Wee, and M. Fornari, “The role of copper in the thermal conductivity of thermoelectric oxychalcogenides: do lone pairs matter?” *Physical Chemistry Chemical Physics* **17**, 31735 (2015).
- [31] N. Ma, Y.-Y. Li, L. Chen, and L.-M. Wu, “ $\alpha$ -CsCu<sub>5</sub>Se<sub>3</sub>: discovery of a low-cost bulk selenide with high thermoelectric performance,” *Journal of the American Chemical Society* **142**, 5293 (2020).
- [32] F. Li, X. Liu, N. Ma, Y.-C. Yang, J.-P. Yin, L. Chen, and L.-M. Wu, “Overdamped phonon diffusion and nontrivial electronic structure leading to a high thermoelectric figure of merit in KCu<sub>5</sub>Se<sub>3</sub>,” *Journal of the American Chemical Society* (2023).
- [33] Y. Shi, A. Assoud, S. Ponou, S. Lidin, and H. Kleinke, “A new material with a composite crystal structure causing ultralow thermal conductivity and outstanding thermoelectric properties: Tl<sub>2</sub>Ag<sub>12</sub>Te<sub>7+</sub>  $\delta$ ,” *Journal of the American Chemical Society* **140**, 8578 (2018).
- [34] A. J. Rettie, J. Ding, X. Zhou, M. J. Johnson, C. D. Malliakas, N. C. Osti, D. Y. Chung, R. Osborn, O. Delaire, S. Rosenkranz, *et al.*, “A two-dimensional type i superionic conductor,” *Nature Materials* **20**, 1683 (2021).
- [35] Z. Feng, T. Jia, J. Zhang, Y. Wang, and Y. Zhang, “Dual effects of lone-pair electrons and rattling atoms in CuBiS<sub>2</sub> on its ultralow thermal conductivity,” *Physical Review B* **96**, 235205 (2017).
- [36] F. Knoop, T. A. Purcell, M. Scheffler, and C. Carbogno, “Anharmonicity measure for materials,” *Physical Review Materials* **4**, 083809 (2020).
- [37] F. Knoop, T. A. Purcell, M. Scheffler, and C. Carbogno, “Anharmonicity in thermal insulators: An analysis from first principles,” *Physical Review Letters* **130**, 236301 (2023).
- [38] L. Chen, H. Tran, R. Batra, C. Kim, and R. Ramprasad, “Machine learning models for the lattice thermal conductivity prediction of inorganic materials,” *Computational Materials Science* **170**, 109155 (2019).
- [39] J. Brightwell, L. Miller, A. Munday, and B. Ray, “The silver iodide–thallium iodide pseudo-binary system,” *Physica Status Solidi (a)* **79**, 293 (1983).
- [40] A. Sdiiraldi, A. Magistris, and E. Pezzati, “Transport processes in TII and in the AgI-TII-system,” *Zeitschrift für Naturforschung A* **29**, 782 (1974).
- [41] U. Aseginolaza, R. Bianco, L. Monacelli, L. Paulatto, M. Calandra, F. Mauri, A. Bergara, and I. Errea, “Phonon collapse and second-order phase transition in thermoelectric SnSe,” *Physical Review Letters* **122**, 075901 (2019).
- [42] O. Hellman, I. Abrikosov, and S. Simak, “Lattice dynamics of anharmonic solids from first principles,” *Physical Review B* **84**, 180301 (2011).
- [43] O. Hellman, P. Steneteg, I. A. Abrikosov, and S. I. Simak, “Tem-

- perature dependent effective potential method for accurate free energy calculations of solids,” *Physical Review B* **87**, 104111 (2013).
- [44] T. Feng and X. Ruan, “Quantum mechanical prediction of four-phonon scattering rates and reduced thermal conductivity of solids,” *Physical Review B* **93**, 045202 (2016).
- [45] T. Feng, L. Lindsay, and X. Ruan, “Four-phonon scattering significantly reduces intrinsic thermal conductivity of solids,” *Physical Review B* **96**, 161201 (2017).
- [46] D. Olives, J. Turcotte, J. Rivet, and J. Flahaut, “Etude structurale et diagrammes de phases des systemes AgI-InI et AgI-InI<sub>3</sub>,” (1972).
- [47] G. Kresse and J. Furthmüller, “Efficient iterative schemes for ab initio total-energy calculations using a plane-wave basis set,” *Physical Review B* **54**, 11169 (1996).
- [48] G. Kresse and D. Joubert, “From ultrasoft pseudopotentials to the projector augmented-wave method,” *Physical Review B* **59**, 1758 (1999).
- [49] A. Pfitzner, M. Evain, and V. Petricek, “Cu<sub>12</sub>Sb<sub>4</sub>S<sub>13</sub>: A temperature-dependent structure investigation,” *Acta Crystallographica Section B: Structural Science* **53**, 337 (1997).
- [50] A. Togo and I. Tanaka, “First principles phonon calculations in materials science,” *Scripta Materialia* **108**, 1 (2015).
- [51] D. A. Keen, “Disordering phenomena in superionic conductors,” *Journal of Physics: Condensed Matter* **14**, R819 (2002).
- [52] W. Li, J. Carrete, N. A. Katcho, and N. Mingo, “ShengBTE: A solver of the boltzmann transport equation for phonons,” *Computer Physics Communications* **185**, 1747 (2014).
- [53] Z. Zeng, C. Zhang, Y. Xia, Z. Fan, C. Wolverton, and Y. Chen, “Nonperturbative phonon scatterings and the two-channel thermal transport in Tl<sub>3</sub>VSe<sub>4</sub>,” *Physical Review B* **103**, 224307 (2021).
- [54] E. Di Lucente, M. Simoncelli, and N. Marzari, “Crossover from boltzmann to wigner thermal transport in thermoelectric skutterudites,” *arXiv preprint arXiv:2303.07019* (2023).
- [55] J. Klarbring, O. Hellman, I. A. Abrikosov, and S. I. Simak, “Anharmonicity and ultralow thermal conductivity in lead-free halide double perovskites,” *Physical Review Letters* **125**, 045701 (2020).
- [56] A. Pogodin, M. Filep, V. Y. Izai, O. Kokhan, and P. Kúš, “Crystal growth and electrical conductivity of Ag<sub>7</sub>PS<sub>6</sub> and Ag<sub>8</sub>GeS<sub>6</sub> argyrodites,” *Journal of Physics and Chemistry of Solids* **168**, 110828 (2022).
- [57] G. J. Snyder and E. S. Toberer, “Complex thermoelectric materials,” *Nature Materials* **7**, 105 (2008).
- [58] Z. Fan, H. Wang, Y. Wu, X. Liu, and Z. Lu, “Thermoelectric high-entropy alloys with low lattice thermal conductivity,” *Rsc Advances* **6**, 52164 (2016).
- [59] Z. Zeng, C. Zhang, H. Yu, W. Li, Y. Pei, and Y. Chen, “Ultralow and glass-like lattice thermal conductivity in crystalline BaAg<sub>2</sub>Te<sub>2</sub>: Strong fourth-order anharmonicity and crucial diffusive thermal transport,” *Materials Today Physics* **21**, 100487 (2021).
- [60] B. H. Toby, “ExpGui, a graphical user interface for gsas,” *Journal of Applied Crystallography* **34**, 210 (2001).
- [61] G. M. Sheldrick, “A short history of shelx,” *Acta Crystallographica Section A: Foundations of Crystallography* **64**, 112 (2008).
- [62] L. J. Bourhis, O. V. Dolomanov, R. J. Gildea, J. A. Howard, and H. Puschmann, “The anatomy of a comprehensive constrained, restrained refinement program for the modern computing environment—olex2 dissected,” *Acta Crystallographica Section A: Foundations and Advances* **71**, 59 (2015).
- [63] U. t. Zucker and H. Schulz, “Statistical approaches for the treatment of anharmonic motion in crystals. i. a comparison of the most frequently used formalisms of anharmonic thermal vibrations,” *Acta Crystallographica Section A: Crystal Physics, Diffraction, Theoretical and General Crystallography* **38**, 563 (1982).
- [64] A. v. d. Lee, F. Boucher, M. Evain, and R. Bree, “Temperature dependence of the silver distribution in Ag<sub>2</sub>MnP<sub>2</sub>S<sub>6</sub> by single crystal x-ray diffraction,” *Zeitschrift für Kristallographie-Crystalline Materials* **203**, 247 (1993).
- [65] F. Boucher, M. Evain, and R. Brec, “Single-crystal structure determination of  $\gamma$ -Ag<sub>8</sub>Si<sub>4</sub>Te<sub>6</sub> and powder X-ray study of low-temperature  $\alpha$  and  $\beta$  phases,” *Journal of Solid State Chemistry* **100**, 341 (1992).
- [66] J. P. Perdew, A. Ruzsinszky, G. I. Csonka, O. A. Vydrov, G. E. Scuseria, L. A. Constantin, X. Zhou, and K. Burke, “Restoring the density-gradient expansion for exchange in solids and surfaces,” *Physical Review Letters* **100**, 136406 (2008).
- [67] F. Eriksson, E. Fransson, and P. Erhart, “The hiphive package for the extraction of high-order force constants by machine learning,” *Advanced Theory and Simulations* **2**, 1800184 (2019).
- [68] T. Tadano and S. Tsuneyuki, “Quartic anharmonicity of rattlers and its effect on lattice thermal conductivity of clathrates from first principles,” *Physical Review Letters* **120**, 105901 (2018).